Advanced Powder Technology 32 (2021) 2336–2344

Contents lists available at ScienceDirect

Advanced Powder Technology

journal homepage: www.elsevier.com/locate/apt

Original Research Paper

# Effect of particle size distribution on hydrodynamics of pneumatic conveying system based on CPFD simulation

Woo Chang Sung [a], Jun Young Kim [a,b,*], Seok Woo Chung [c], Dong Hyun Lee [a,*]

[a] School of Chemical Engineering, Sungkyunkwan University, 2066 Seobu-Ro, Jangan, Suwon 16419, Republic of Korea
[b] Institute of Convergent Chemical Engineering and Technology, Sungkyunkwan University, 2066 Seobu-Ro, Jangan, Suwon 16419, Republic of Korea
[c] Institute for Advanced Engineering, Goan-ro 51beon-gil, Baegam-myeon, Cheoin-gu, Yongin 17528, Republic of Korea

ARTICLE INFO

*Article history:*
Received 16 January 2021
Received in revised form 17 April 2021
Accepted 3 May 2021
Available online 27 May 2021

*Keywords:*
Horizontal pneumatic conveying
CPFD simulation
Particle size distribution
Drag force coefficient
Sauter mean diameter

ABSTRACT

The effect of particle size distribution on the hydrodynamics of dilute-phase pneumatic conveying system was analyzed using computational particle fluid dynamics (CPFD) simulation. The influence of a simulation parameter, i.e., correction factor of drag coefficient ($k$), on the hydrodynamics of pneumatic conveying system was determined *via* CPFD simulation. When results of simulation were compared with experimental data of previous studies, the average error of pressure drop per length predicted by the CPFD approach with the correction factor was below 4.4%. Saltation velocity and the pressure drop per unit length declined as the drag force coefficient increased. Simulation results also revealed that the pressure drop per length and the saltation velocity were decreased when the fine powder fraction in the particle size distribution was increased, although the width of particle size distribution was widened, and the standard deviation was increased. Finally, the Relative Standard Deviation (RSD) of pressure drop per length was measured and compared with median diameter ($d_{50}$), Sauter mean diameter, geometric mean diameter, and arithmetic mean diameter. The RSD of the Sauter mean diameter was 5.8%, approximately twice less than the RSD value of $d_{50}$ commonly used in pneumatic conveying.


## 1. Introduction

A pneumatic conveying system is widely used in various industries such as agriculture, chemical manufacture, pharmaceuticals, paints, mining, mineral processing, rubber, and electric power generation [1–6] due to its many advantages such as dust-free transportation, particle transmission via horizontal and vertical pipelines, and particle transportation by bending sections into various shapes. In addition, the cost of maintaining the pneumatic conveying system is relatively low. Thus, this system can be used to transport valuable materials safely at no additional cost [7,8]. This system is also relatively easy to automate and control [3]. Nonetheless, the prediction of gas–solid flow behavior and the interaction between particles and walls are complex. Furthermore, several studies have reported effects of particle parameters such as sphericity, particle size, particle density, and particle–wall interactions such as particle wall adhesion and wall roughness on hydrodynamics of pneumatic conveying system using Computational Fluid Dynamics (CFD) [9–13]. Thus, the pneumatic conveying system needs to consider these fluidization behavior, as well as particle properties, to construct the system [14].

The pneumatic system has recently attracted increased attention for transportation of offshore drillings. Following offshore drilling operations, the particle size generally shows a wide distribution ranging from 100 to 2000 μm [15]. Although the particle size significantly affects saltation velocity during particle transmission, to the authors' best knowledge, the effect of particle size distribution (PSD) on pneumatic conveying system has not been investigated comprehensively yet [14]. Until now, the empirical correlations for the pneumatic conveying system have been developed using the median diameter ($d_{50}$) representing the PSD. The particle size was considered uniform during CFD simulation of the pneumatic system [16–19]. Although the role of PSD in a pneumatic conveying system has yet to be reported, studies have investigated changes in pick-up velocity when two solid species are combined [20]. The variance in the PSD of a pneumatic conveying system may alter the flow regime under the same flow rate, thus affecting operating conditions. CFD and Discrete Element Method (DEM) are usually not appropriate for determining the effect of PSD due to a high computational cost [21–23]. Compared with CFD or DEM simulations, Computational Particle Fluid

* Corresponding authors.
*E-mail addresses:* june0112@g.skku.edu (J.Y. Kim), dhlee@skku.edu (D.H. Lee).

https://doi.org/10.1016/j.apt.2021.05.010
0921-8831/

**Nomenclature**

| | |
|---|---|
| $A_p$ | Acceleration of particle, [m/s$^2$] |
| $Ar$ | Archimedes number, [–] |
| $C_d$ | Drag coefficient, [–] |
| $D$ | Combined drag function, [1/s] |
| $D_1$ | Wen and Yu drag function, [1/s] |
| $D_2$ | Ergun drag function, [1/s] |
| $\overline{D_p}$ | Average particle drag function, [1/s] |
| $D_p$ | Drag function at the particle location, [1/s] |
| $D_t$ | Internal diameter of pipe, [mm] |
| $D_{t,50}$ | Internal pipe with a diameter of 50 mm [mm] |
| $d_i$ | Particle diameter of bin i, [μm] |
| $d_{10}$ | 10 percentile diameter, [μm] |
| $d_{50}$ | Median diameter, [μm] |
| $d_{90}$ | 90 percentile diameter, [μm] |
| $d_i$ | Diameter of i$^{th}$ particle, [μm] |
| $d_{sv}$ | Sauter mean diameter, [μm] |
| $d_{go}$ | Geometric mean diameter, [μm] |
| $d_{ar}$ | Arithmetic mean diameter, [μm] |
| $F$ | Momentum transfer between the fluid and solid phases, [N] |
| $f$ | Probability distribution function derived from Liouville's equation, [–] |
| $g$ | Acceleration due to gravity, [m/s$^2$] |
| $g_1$ | Blending function introduced by Peter et al. [31], [–] |
| $k$ | Correction factor of drag coefficient, [–] |
| $n$ | Superficial gas velocity designated point, [–] |
| $n_i$ | Number of particles in bin i, [–] |
| $p$ | Fluid pressure, [Pa] |
| $p_s$ | Solid pressure in Eulerian CFD; positive constant for particle normal stressinCPFD [Pa] |
| $\frac{\Delta P}{L}$ | Pressure drop per length, [Pa/m] |
| $Re$ | Reynolds number, [–] |
| $r_n$ | Normal-to-wall momentum retention, [–] |
| $r_p$ | Radius of particle, [μm] |
| $r_t$ | Tangent-to-wall momentum retention, [–] |
| $S_i$ | Standard deviation of particle size distribution designated point, [–] |
| $u_f$ | Gas phase velocity, [m/s] |
| $u_g$ | Superficial gas velocity, [m/s] |
| $u_p$ | Solid phase velocity, [m/s] |
| $\bar{u}_P$ | Drag-averaged particle velocity, [m/s] |
| $u_{p,n}$ | Velocity of N$^{th}$ particle, [m/s] |
| $V_p$ | Particle volume, [m$^3$] |
| $X_p$ | Modified acceleration due to constant stresses, [m/s$^2$] |
| $X_j$ | Superficial gas velocity designated point, [–] |
| $x_p$ | Particle position, [m] |

*Greek symbols*

| | |
|---|---|
| $\varepsilon$ | Constant of inter-particle normal stress, [–] |
| $\beta$ | Constant of inter-particle normal stress, [–] |
| $\theta_{cp}$ | Particle volume fraction when particle is packed, [–] |
| $\theta_p$ | Particle volume fraction, [–] |
| $\theta_f$ | Fluid volume fraction, [–] |
| $\rho_f$ | Fluid density, [kg/m$^3$] |
| $\rho_p$ | Particle density, [kg/m$^3$] |
| $\bar{\rho}_p$ | Mass-averaged particle density, [kg/m$^3$] |
| $\tau_f$ | Fluid stress tensor, [Pa] |
| $\tau_p$ | Inter-particle normal stress, [Pa] |

*Subscripts*

| | |
|---|---|
| f | Fluid |
| p | Particle |

Dynamics (CPFD) enables calculation of a wider PSD using the MP-PIC (Multiphase Particle-in cell) method [22,24–27]. Thus, CPFD simulation was used to confirm hydrodynamic changes in the pneumatic conveying system according to changes in PSD. Barracuda®, a commercial code for CPFD simulation was used in this study.

CPFD has been investigated in many fields, but rarely in pneumatic conveying [28–30]. In case of a dense phase involving a vertical pneumatic conveying system, CPFD simulation can adequately predict actual experimental results [30]. In case of a dilute phase in a horizontal pneumatic conveying system, effects of simulation parameters (normal-to-wall momentum retention ($r_n$) and tangent-to-wall momentum retention ($r_t$)) of CPFD simulation have been confirmed. When the retention value of particle wall momentum is 0.98, the simulation can adequately predict a diluted horizontal pneumatic conveying system, similar to actual experimental results [29,30]. However, the effect of drag force on simulation has not been analyzed and a pneumatic conveying system using CPFD simulation has yet to be interpreted.

Therefore, effects of drag force coefficient and PSD on the hydrodynamics of a horizontal pneumatic conveying system were investigated in this study and the appropriate value of drag force coefficient was determined. Furthermore, four types of average particle size based on median diameter ($d_{50}$), Sauter mean diameter ($d_{sv}$), geometric mean diameter ($d_{go}$), and arithmetic mean diameter ($d_{ar}$) for the pneumatic conveying system were compared with calculated values of relative standard deviation (RSD) following CPFD simulation in order to select the appropriate particle diameter.

## 2. Modeling

### 2.1. Governing equations for CPFD

The CPFD method was used to calculate the three-dimensional momentum of particles and fluids. The fluid phase was calculated using the Navier-Stokes equation, while the discrete solid phase was determined by grouping similar particles into cells using a Multi-Phase Particle-In-Cell (MP-PIC) numerical method. Both fluid and solid phases were coupled with the interphase drag force [21].

The governing equation varied with fluid and particle phases. The fluid phase was calculated using Eq. (1):

$$\frac{\partial}{\partial t}\left(\rho_f\theta_f\right)+\nabla\cdot\left(\rho_f\theta_f u_f\right)=0 \tag{1}$$

The momentum of the incompressible fluid was calculated using Eq. (2):

$$\frac{\partial}{\partial t}\left(\rho_f\theta_f u_f\right)+\nabla\cdot\left(\rho_f\theta_f u_f u_f\right)=-\nabla p-F+\rho_f\theta_f g+\nabla\cdot\left(\theta_f\tau_f\right) \tag{2}$$

In Eq. (2), $\rho_f$ was fluid density, $\theta_f$ was fluid volume fraction, $u_f$ was fluid velocity, $p$ was fluid pressure, $\tau_f$ was fluid stress tensor, $g$ was acceleration of gravity, and $F$ was the rate of momentum exchange per volume between fluid and particle phases:

$$F=\iiint fV_p\rho_p\left[D_p\left(u_f-u_p\right)-\frac{1}{\rho_p}\nabla p\right]dV_p d\rho_p du_p \tag{3}$$

where $V_p$ was particle volume, $u_p$ was particle velocity, $\rho_p$ was particle density, $D_p$ was the drag function at the particle location, and $f$

was the distribution function calculated using the Liouville's equation [21].

Particles were analyzed via Eq. (4) using the Lagrangian method:

$$A_p = \frac{d(u_p)}{dt} = D_p(u_f - u_p) - \frac{\nabla p}{\rho_p} + X_p + g \tag{4}$$

In the modified stress term ($X_p$), individual particle acceleration represented a blend between particle acceleration and the original MP-PIC method, which was appropriate for rapid granular flow (the first term on the right-hand side of Eq. (5)) and the average particle acceleration in a close-packed state.

$$X_p = -\frac{\nabla \tau_p}{\bar{\rho}_p \theta_p} + g_1(\theta_p)[\bar{D}_p\left(u_f - \bar{u}_p\right) - D_p(u_f - u_p) - (\frac{1}{\bar{\rho}_p} - \frac{1}{\rho_p})\nabla p \tag{5}$$

The term $\bar{u}_P$in Eq. (5) represented the drag-averaged particle velocity and $\bar{\rho}_p$was the mass-averaged particle density. The term $g_1$denoted the blending function introduced by Peter *et al.* [31]. Eqs. (4) and (5) represented aerodynamic drag, in which $\tau_p$ denoted inter-particle normal stress expressed in Eq. (6):

$$\tau_p = \frac{p_s \theta_p^{\beta}}{\max[(\theta_{cp} - \theta_p), \varepsilon(1 - \theta_p)]} \tag{6}$$

where$\varepsilon$In Eq. (6), $\varepsilon$ where$\varepsilon$was a small numerical constant denoting inter-particle normal stress. It was used to calibrate when particles were closely packed. In this study, the value of $\varepsilon$where$\varepsilon$ was about $10^{-7}$. The constant $p_s$ was expressed in units of pressure. It was also used to calibrate the value of $\tau_p$. $\theta_{\mathrm{cp}}\theta_{cp}$ represented the fraction of particle volume when particles were packed. $\beta$ was also a constant indicating inter–particle normal stress, with a value normally ranging from 2 to 5 and a default value of 3. Since the value of $\theta_{\mathrm{p}}\theta_p$ does not reach $\theta_{cp}\theta_{\mathrm{cp}}$, the value of $\tau$ is not generally large [32]. Thus, the particle–particle interaction did not have a relatively large effect.

The particle position was calculated using Eq. (7):

$$\frac{dx_p}{dt} = u_p \tag{7}$$

### 2.2. Drag models

Wen and Yu correlation [33] is known to generally fit well with a dilute system while the Ergun equation [34] is appropriate for packed particles. Gidaspow [35] has proposed a drag function by combining these two expressions. The combined drag function is expressed as:

$$D_p = \begin{cases} D_1 & \theta_p < 0.75\theta_{cp} \\ (D_2 - D_1)(\frac{\theta_p - 0.75\theta_{cp}}{0.85\theta_{cp} - 0.75\theta_{cp}}) + D_1 & 0.85\theta_{cp} \geq \theta_p \geq 0.75\theta_{cp} \\ D_2 & \theta_p > 0.85\theta_{cp} \end{cases} \tag{8}$$

In Eq. (8), $\theta_p$ represents the volume fraction of the particle, $\theta_{cp}$ is the volume fraction of close packed state, and $D_1$ refers to the value derived from the Wen and Yu drag model [33] based on Eq. (9):

$$D_1 = \frac{3}{8} C_d \frac{\rho_f |u_f - u_p|}{\rho_p r_p} \tag{9}$$

$C_{\mathrm{d}}$ represents the drag coefficient in the Wen and Yu equation:

$$C_d = \begin{cases} k \times \frac{24}{Re} \times \theta_f^{-2.65} & Re < 0.5 \\ k \times \frac{24}{Re} \times \theta_f^{-2.65}(1 + 0.15Re^{0.687}) & 0.5 \leq Re \leq 1000 \\ k \times 0.44 \times \theta_f^{-2.65} & Re > 1000 \end{cases} \tag{10}$$

The constant $k$ is a correction factor of drag coefficient used to increase or decrease the value of $C_d$ to fit experimental data [36].

The Ergun equation can be expressed as Eq. (11):

$$D_2 = 0.5\left(\frac{180 \times \theta_p}{\theta_f Re} + 2\right)\frac{\rho_f |u_f - u_p|}{\rho_p r_p} \tag{11}$$

## 3. Simulation set-up

Geometry, particle properties, and operating conditions were similar to those in previous experiments [30]. The fluid flow was isothermal and incompressible. Effects of gravity were considered. Note that no chemical reaction was included here as the system was designed to transfer materials, not to act as a reactor.

### 3.1. Geometry and grid resolution

The pneumatic conveyer used in the previous study [30] had an inlet diameter of 81 mm and a length of 11.5 m. However, as this geometry required prolonged computational time to simulate a pipe, an optimization simulation of the pipe length was conducted. As shown in Supplementary Fig. 1, the particle velocity and volume fraction converged to a constant value less than 1.7% of the relative error of 1.5 m in length. As the particle velocity and particle volume fraction profiles stabilized at approximately 1.5 m, the pipe length was set to be 3 m for CPFD simulation.

The geometry was meshed with a built-in module in Barracuda® software as shown in Fig. 1. The mesh consisted of 765,625 cells (35 × 35 × 525) in total, with each cell measuring 2.3 × 2.3 × 5.7 mm in size. Here, the resolution of the grid was selected following a mesh independence test as described in Fig. 2. When the grid resolution was less than 20 × 20 × 525, the pressure drop per length was underestimated, implying that the simulation did not accurately reflect the wall effect. When the grid resolution was greater than 20 × 20 × 525, the value of pressure drop per length converged to less than 1.7% of the relative error as shown in Fig. 2. Thus, the grid resolution was selected as 35 × 35 × 525. The computational time was approximately 24 h with a grid resolution of 35 × 35 × 525. Specifications used for the simulation were Intel® I7-8700K & NVIDIA Titan XP, RAM 32 GB).

### 3.2. Material properties

Particle characteristics were similar to those reported in a previous study [30], including a particle density of 2,715 kg/m$^3$ and a $d_{50}$ of 290 μm. To evaluate the effect of PSD on the hydrodynamics of the pneumatic conveying system, the width of PSD was changed. Selection of appropriate PSD function is necessary in order to eliminate the shape effect. Many previous studies have used log normal distribution as a PSD [37–43]. Furthermore, the sample size of drill cuttings followed a log normal distribution. In this study, $d_{50}$ was fixed at 290 μm. The standard deviation of log normal distribution, i.e., the width of PSD was altered as depicted in Fig. 3.

To determine the most appropriate type of particle mean diameter in the pneumatic conveying system, the PSD was changed while fixing each type of particle mean diameter constant as shown in Table 1. The width of PSD was changed by selecting different standard deviations of log normal diameter distribution, while one of these mean particle sizes based on four different parameters (i.e., $d_{50}$, $d_{sv}$, $d_{go}$ and $d_{ar}$) was held constant.

### 3.3. Initial and boundary conditions

The initial air flow was set in the absence of particles, assuming that the initial pressure inside the pneumatic conveyer was set to

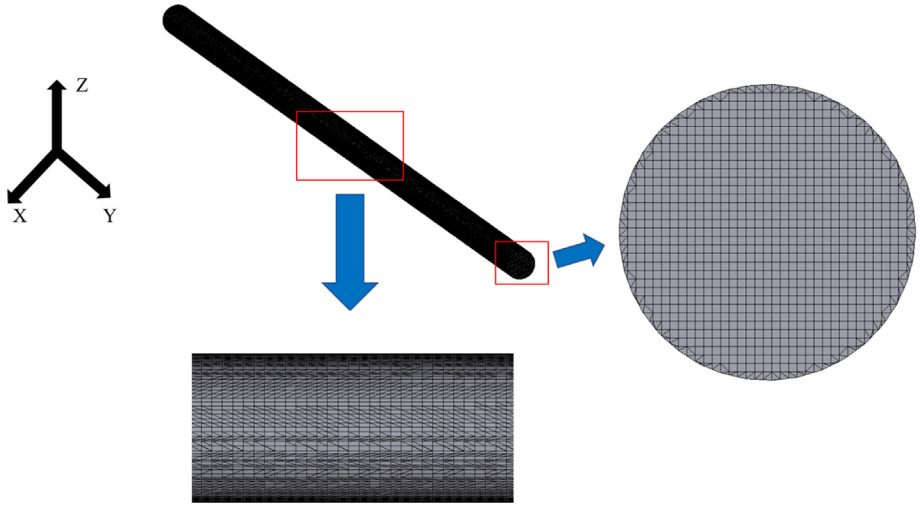


**Fig. 1.** The computational domain of geometry.

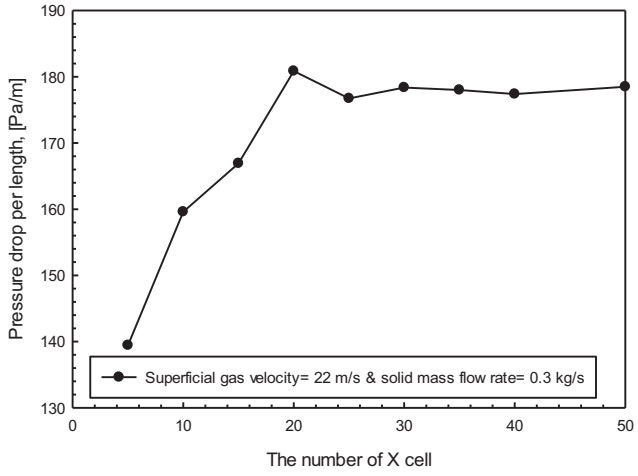


**Fig. 2.** Pressure drop per length under a changing grid resolution. Superficial gas velocity was set to be 22 m/s and solid mass flow rate was set at 0.3 kg/s.

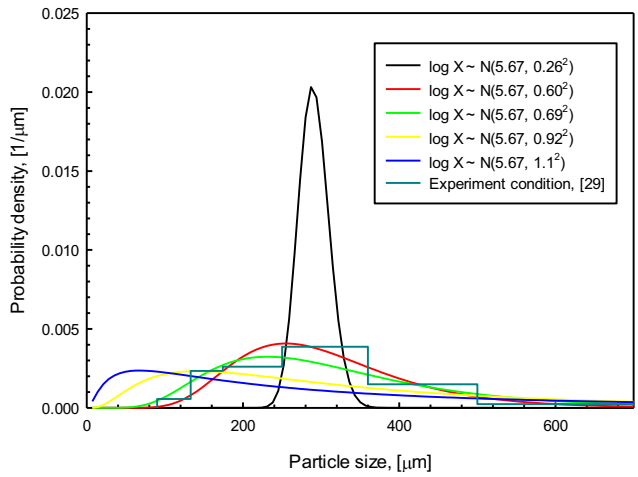


**Fig. 3.** Particle size distribution vs. particle size distribution variance.

be 1 atm of air without particles. The superficial gas velocity ranged from 14.8 to 30 m/s. The air density was 1.2 kg/m$^3$ and the temperature was fixed at 298 K. The outlet pressure was maintained at atmospheric pressure (101325 Pa). The inlet pressure varied with pressure variance in the pneumatic conveying pipe. The initial particle velocity at the inlet boundary was set to be 0. The solid mass feed rate was fixed at 0.3 kg/s, similar to previous experimental conditions [30]. A bounce-back condition was used to model particle–wall interactions, assuming that 95% of normal and 98% of the tangential momentum of particles were retained after collision with the pipe wall, i.e., a normal-to-wall momentum retention ($r_n$) = 0.95, and a tangent-to-wall momentum retention ($r_t$) = 0.98 in the Barracuda set-up. These values were confirmed to be appropriate under simulation conditions [29,30].

### 3.4. Simulation time and convergence criterion

The simulation was calculated in a transient state. The initial time step was set to be 0.0001 s. However, the time step was adjusted with the mesh and parcel for the computational accuracy using the Barracuda Courant-Friedrichs-Lewy (CFL) algorithm [44]. The lower and upper limits of the CFL algorithm were set to be 0.8 and 1.5, respectively. To ensure a steady state of simulation, the pressure drop per length was determined over time. Pressure drop per length was calculated from 2.5 m to 3 m of length. After 1 s, as shown in Fig. 4, the pressure drop per length was converged to a constant value, less than 1.3% of the relative error. Based on these results, the simulation time was set to be 3 s. Limited residual values for convergence were set to be $10^{-7}$, $10^{-8}$, and $10^{-7}$ for volume, pressure, and velocity, respectively. A large eddy simulation (LES) was used, in which large eddies were directly calculated. The subgrid-scale (SGS) turbulence was calculated using the Smagorinsky method [45].

## 4. Results and discussion

### 4.1. Drag force coefficient

Although the value of the correction factor of drag coefficient ($k$) commonly used in Barracuda® is 1, many previous studies have reported that this value may differ depending on experimental conditions [46–48]. A previous study of a circulating fluidized bed similar to the pneumatic conveying system has shown that a $k$ value of 0.7 fits well [47]. In addition, the Wen & Yu-Ergun drag model, which was used in this study, overestimated the drag force in a circulating fluidized bed riser under CPFD simulation [49]. Therefore, the effect of $k$ on simulation was confirmed and

**Table 1**
Particle size distribution in cases showing log normal distribution (log X ~ N (μ, $\sigma^2$), *d*:μm).

| Item | μ | σ | $d_{10}$ | $d_{50}$ | $d_{90}$ | $d_{sv}$ | $d_{go}$ | $d_{ar}$ |
|---|---|---|---|---|---|---|---|---|
| Case 1 | 5.67 | 0 | 290 | 290 | 290 | 290 | 290 | 290 |
| Case 2 | 5.67 | 0.26 | 207 | 290 | 406 | 281 | 291 | 301 |
| Case 3 | 5.67 | 0.6 | 135 | 290 | 625 | 248 | 295 | 349 |
| Case 4 | 5.67 | 0.69 | 119 | 290 | 705 | 235 | 296 | 372 |
| Case 5 | 5.67 | 0.92 | 90 | 290 | 938 | 201 | 301 | 445 |
| Case 6 | 5.67 | 1.1 | 71 | 290 | 1186 | 172 | 306 | 532 |
| Case 7 | 5.3 | 0 | 201 | 201 | 201 | 201 | 201 | 201 |
| Case 8 | 5.33 | 0.26 | 148 | 207 | 290 | 201 | 208 | 215 |
| Case 9 | 5.46 | 0.6 | 109 | 235 | 507 | 201 | 239 | 284 |
| Case 10 | 5.51 | 0.69 | 102 | 248 | 603 | 201 | 253 | 318 |
| Case 11 | 5.67 | 0.92 | 90 | 290 | 938 | 201 | 301 | 445 |
| Case 12 | 5.83 | 1.1 | 83 | 340 | 1391 | 201 | 359 | 624 |
| Case 13 | 5.7 | 0 | 300 | 300 | 300 | 300 | 300 | 300 |
| Case 14 | 5.7 | 0.26 | 214 | 300 | 420 | 291 | 300 | 311 |
| Case 15 | 5.69 | 0.6 | 137 | 296 | 637 | 253 | 300 | 357 |
| Case 16 | 5.68 | 0.69 | 121 | 294 | 715 | 239 | 300 | 377 |
| Case 17 | 5.67 | 0.92 | 90 | 290 | 938 | 201 | 300 | 445 |
| Case 18 | 5.65 | 1.1 | 70 | 285 | 1167 | 169 | 300 | 524 |
| Case 19 | 6.1 | 0 | 444 | 444 | 444 | 444 | 444 | 444 |
| Case 20 | 6.06 | 0.26 | 306 | 428 | 600 | 416 | 430 | 444 |
| Case 21 | 5.91 | 0.6 | 171 | 369 | 794 | 315 | 375 | 444 |
| Case 22 | 5.848 | 0.69 | 143 | 347 | 842 | 281 | 354 | 444 |
| Case 23 | 5.67 | 0.92 | 90 | 290 | 938 | 201 | 301 | 444 |
| Case 24 | 5.49 | 1.1 | 59 | 242 | 990 | 143 | 255 | 444 |

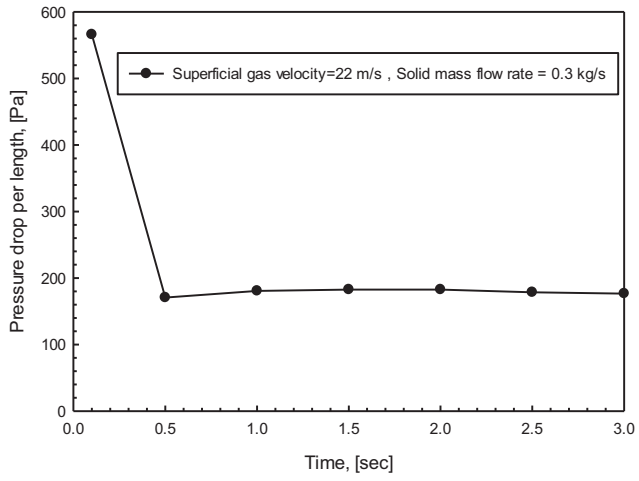


**Fig. 4.** Pressure drop per length over simulation time at $u_g$ of 22 m/s and solid mass flow rate of 0.3 kg/s.

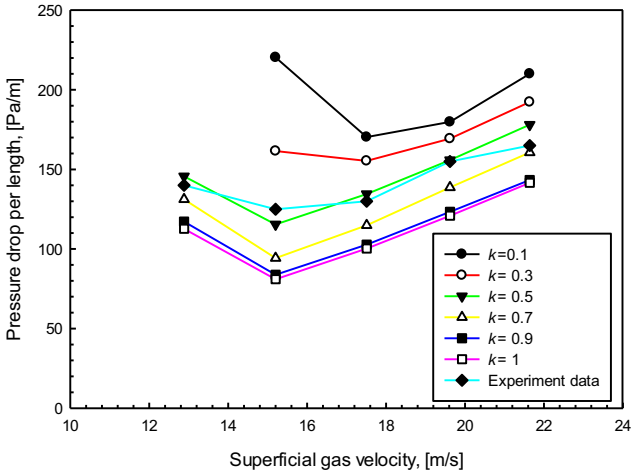


**Fig. 5.** Pressure drop per length with a changing correction factor of drag coefficient and a fixed solid mass flow rate at 0.3 kg/s.

experimental and simulation results were validated by changing the *k* value in the method used in previous studies [50].

The pressure drop per length under various *k* values is depicted in Fig. 5. The pressure drop per length was averaged over time from 2 s to 3 s. Previous experimental data [30] were used to validate simulation results. As expressed in Eq. (10), *k* is a scalar product of the drag force. As the *k* value changed, the value of drag force also varied. In the pneumatic conveying system, the drag force is related to saltation velocity, which refers to the velocity at which the total pressure drop per unit length of the flow is minimum [51–53]. Also, it is the minimum velocity required for conveying solids without formation of stationary beds and dunes at the bottom of the pipe [54]. As demonstrated in previous studies, the saltation velocity where the pressure drop per length changes rapidly (Fig. 5) decreased as the value of k increased. Previous studies have reported that drag force is a significant value of saltation velocity [9,10,54–56]. As the value of *k* increased, the drag force increased the particle velocity as well, but decreased the saltation velocity.

However, the pressure drop per length decreased as the *k* value increased. The slip velocity of a particle is related to the drag force [46] thus increasing the drag force increases the particle velocity. When superficial gas velocity was 21.64 m/s and the solid mass flow rate was set to be 0.3 kg/s, the particle velocity was increased when the *k* value was increased as shown in supplementary Fig. 1 (A). Increasing the particle velocity decreased the particle residence time, which decreased the particle volume fraction inside the pneumatic conveyer as shown in supplementary Fig. 1 (B). As a result, a decrease in *k* value triggered a decrease in pressure drop.

However, when simulation results were compared to experimental results reported in the previous study [30], experimental results of the saltation velocity (the total pressure drop per length becomes minimum) and pressure drop values adequately matched when the *k* value was set to be 0.5 (Fig. 5). Experimental data and simulation results of pressure drop per length with solid mass flow rate fixed at 0.25 or 0.35 kg/s are depicted in supplementary Fig. 2. Likewise, when the *k* value was 0.5, experimental results of the previous study well matched with simulation results.

### 4.2. Effect of particle size distribution

To validate the effect of PSD on the hydrodynamics of the pneumatic conveying system, the simulation was performed assuming a log normal distribution as mentioned in Section 3. Although the median diameter ($d_{50}$) was fixed, the pressure drop per length varied with the width of PSD as shown in Fig. 6. When the particle size was mono-sized (case 1) and the PSD had a narrow distribution (case 2), the saltation velocity, with a huge peak representing the pressure drop per length, was approximately 15 m/s. As expressed in supplementary Fig. 3, under the velocity at which the pressure drop was rapidly decreased, particles accumulated and formed dunes at the bottom of the pipe. Similar to previous studies [51,54,57], before the saltation velocity, some particles were transported in the form of dunes while others were conveyed with the air in pneumatic conveyor. However, when the PSD was wider (cases 3–6), no significant change occurred in the pressure drop per length. In case of mono-sized particles (case 1), some particles were transported to the bottom forming dunes. However, when the PSD was wider (cases 3–6), particles were transported in the dilute regime, even in case 1 and case 6 operated at the same superficial gas velocity (supplementary Fig. 3).

Differences in flow regime despite similar median diameter ($d_{50}$) are explained graphically by plotting particle velocity against PSD (Fig. 7). The particle velocity according to each PSD was based on altered standard deviation as shown in Fig. 7. The particle velocity was determined by calculating the average velocity of particles passing through the pneumatic conveyer:

$$\text{Particle average velocity} = \frac{\sum_{n=1}^{n=n} u_{p,n}}{n} \tag{12}$$

As the PSD grew wider, the average particle velocity gradually increased (Fig. 7) due to two reasons. First, as explained by Coussot and Kaitna *et al.* [58,59], the small particle effect, in which fine particles suspended in the fluid, can alter the effective fluid properties such as density and viscosity. Thus, fine particles are easily accelerated and suspended in air, which further accelerates coarse particles. Results of CPFD simulation showed that the velocity of particles larger than 290 μm (case 6) was greater than the average velocity of single-sized particles in case 1 as shown in supplementary Fig. 4. Second, the average particle velocity was gradually increased as the PSD was widened due to an increase in the total surface area of particles. The total surface area of particles was 1.69-fold larger in case 6, which had the widest PSD, than that in case 1 with a single particle size. As the total surface area of the particles increased, the projected area of the drag force of the air on the particles also increased, resulting in an increase in the average particle velocity [60,61].

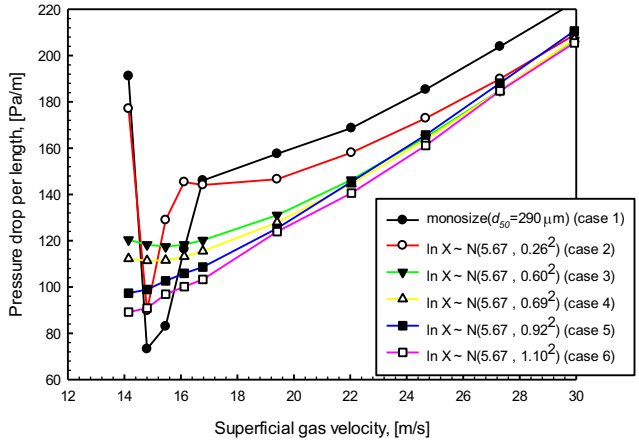


**Fig. 6.** Pressure drop per length with a changing particle size distribution and a fixed solid mass flow rate at 0.3 kg/s.

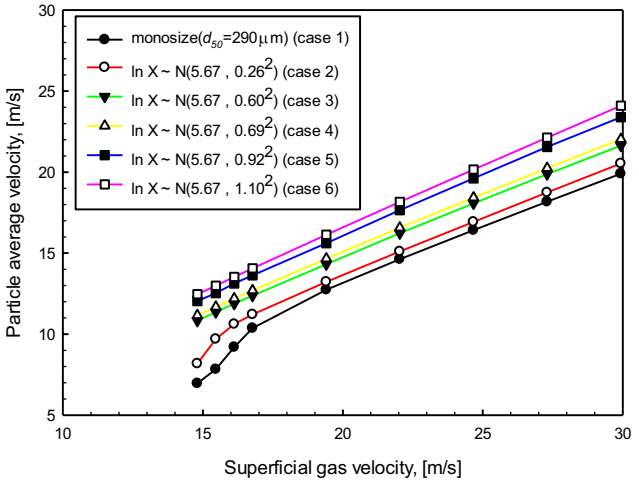


**Fig. 7.** Particle average velocity with a changing particle size distribution is changed and a fixed solid mass flow rate at 0.3 kg/s.

In the dilute regime, particle velocity increased linearly with an increase in superficial gas velocity, similar to the fixed $u_p/u_g$ value regardless of the superficial gas velocity as described previously [62]. However, Santo *et al.* [62] have proposed an empirical correlation for $u_p/u_g$ as follows:

$$\frac{u_p}{u_g} = 1 - 0.02[Ar \times (\frac{\rho_p - \rho_f}{\rho_f}) \times (\frac{D_t}{D_{t,50}})^{-2}]^{0.14} \tag{13}$$

where $Ar$ represents the Archimedes number, $D_t$ denotes inlet diameter of pipe, and $D_{t,50}$ refers to internal pipe diameter of 50 mm. Based on Eq. (13), the value of $u_p/u_g$ was 0.847 when $d_{50}$ was 290 μm. However, when the PSD was changed while the $d_{50}$ was fixed, the value of $u_p/u_g$ showed a significant difference (Table 2), suggesting that the pneumatic conveying system designed with a correlation using $d_{50}$ as a mean diameter might not represent the particle property precisely.

### 4.3. Comparison of various mean particle sizes

In Section 4.2, effects of PSD magnitude on pressure drop per length, $u_p/u_g$, and the average particle velocity were investigated. Unfortunately, several existing correlations did not consider the effect of PSD as a parameter. Instead, they generally calculated pressure drop per length or $u_p/u_g$ based on the average particle size, especially median diameter ($d_{50}$). Thus, most correlations do not represent actual results since large errors can be generated using the $d_{50}$ value, which cannot show PSD variance. To minimize the

**Table 2**
Values of $u_p/u_g$ under altered particle size distribution and constant $d_{50}$.

| Cases | $u_p/u_g$ |
|---|---|
| Case 1 | 0.66 |
| Case 2 | 0.69 |
| Case 3 | 0.73 |
| Case 4 | 0.75 |
| Case 5 | 0.79 |
| Case 6 | 0.82 |

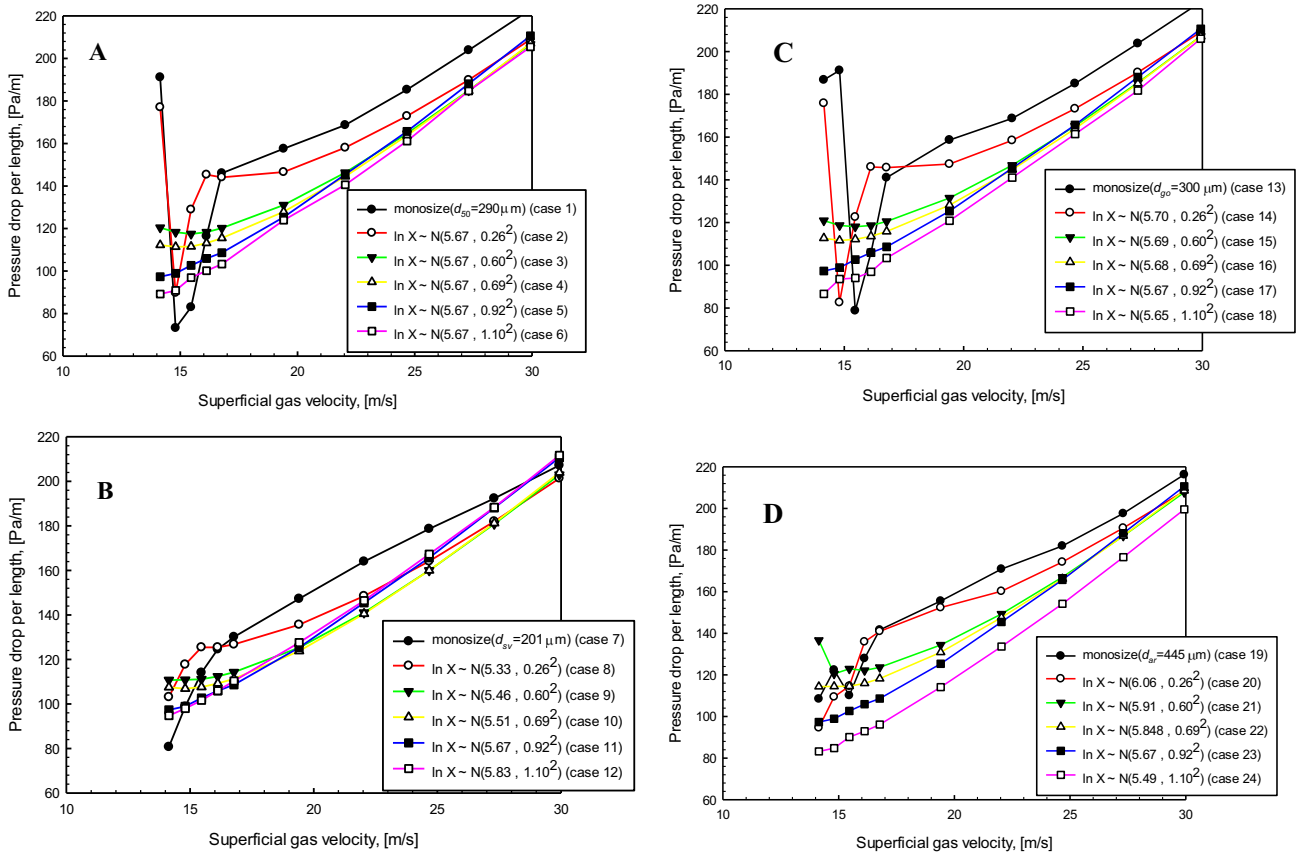


**Fig. 8.** Pressure drop per length under altered particle size distribution, (A) constant $d_{50}$, (B) constant Sauter mean diameter ($d_{sv}$), (C) constant geometric diameter ($d_{go}$), and (D) constant arithmetic diameter ($d_{ar}$) with a fixed solid mass flow rate at 0.3 kg/s.

error involving the previous correlation, it is necessary to confirm the most appropriate particle mean size to express the PSD in the pneumatic conveying system. Therefore, four parameters of average particle size ($d_{50}$, $d_{sv}$, $d_{go}$, and $d_{ar}$) were compared in this study. Under different widths of PSD, cases 2, 8, 14, and 20 showed the same PSD, whereas cases 1 to 6 showed the same $d_{50}$ value. Cases 7 to 12 displayed the same $d_{sv}$ value. Cases 13 to 18 exhibited the same $d_{go}$ value and cases 19 to 24 carried the same $d_{ar}$ as shown in Table 1.

The pressure drop per length was calculated in those cases while changing the superficial gas velocity (Fig. 8). Results of pressure drop per length of cases 1 and 6 differed from those of cases 7 and 12. To quantify such differences, RSD was used. The RSD was calculated by dividing the standard deviation by the average value to indicate data spread [63]. The RSD value of the pressure drop per length according to the PSD width was calculated under the same superficial gas velocity condition. Calculated RSD values for each superficial gas velocity were averaged. It was calculated using the following equation.

$$RSD = \sum_{j=1}^{10}\left(\frac{\sqrt{\frac{\sum_{i=1}^{6}\left(\left(\frac{\Delta P}{L}\right)_{S_i X_j} - \frac{\sum_{i=1}^{6}\left(\frac{\Delta P}{L}\right)_{S_i X_j}}{6}\right)^2}{6}}{\frac{\sum_{i=1}^{6}\left(\frac{\Delta P}{L}\right)_{S_i X_j}}{6}}\right) \times \frac{1}{10} \quad (14)$$

where $X_j$ was the superficial gas velocity of the designated point (specifically, $X_1$ = 14.1435 m/s, $X_2$ = 14.8 m/s, …,$X_9$ = 27.3 m/s, $X_{10}$ = 29.9 m/s, Fig. 8) and $S_i$ was the standard deviation of PSD of the designated point (specifically $S_1$ = 0, $S_2$ = 0.26, …, $S_5$ = 0.92, $S_6$ = 1.1). If the average particle size accurately represented the PSD, the pressure drop per unit length should be similar to the case with the same average particle size but different PSD magnitude. Thus, the smaller the RSD of the pressure drop per length, the better the average particle size representing the entire PSD. The RSD of the pressure drop per length according to the PSD magnitude was calculated for different cases under a constant superficial gas velocity and an average particle size ($d_{50}$: case 1–6, $d_{sv}$: case 7–12, $d_{go}$: case 13–18, $d_{ar}$: case 19–24). The RSD of pressure drop per length was calculated and averaged by varying superficial gas velocities (14 m/s–30 m/s).

The RSD calculated above is shown in Fig. 9. It was found that the $d_{sv}$ of an average particle showed less error with the PSD magnitude. Compared with $d_{50}$ conventionally used for the pneumatic conveying system, it was found that the error was about twice larger than the $d_{sv}$ under the same simulation conditions ($u_g$ = 14–30 m/s and solid mass flow rate = 0.3 kg/s). Compared with $d_{sv}$, the effect of fine particles was underestimated based on $d_{50}$. However, the $d_{sv}$ was obtained by dividing the particle volume by the particle surface using the following equation [64,65]:

$$d_{sv} = \frac{\sum_{i=1}^{n} n_i d_i^3}{\sum_{i=1}^{n} n_i d_i^2} \quad (15)$$

where $n_i$ and $d_i$ were particle number and diameter, respectively. The Sauter mean diameter of spherical objects reflects the size and the total surface energy of the objects is equal to the average surface energy of dispersed particles [66]. Therefore, the Sauter mean diameter reflects the effect of fine particles with a large surface area relative to the same volume. However, the particle flow of the fluid is greatly affected by the drag force between the fluid and

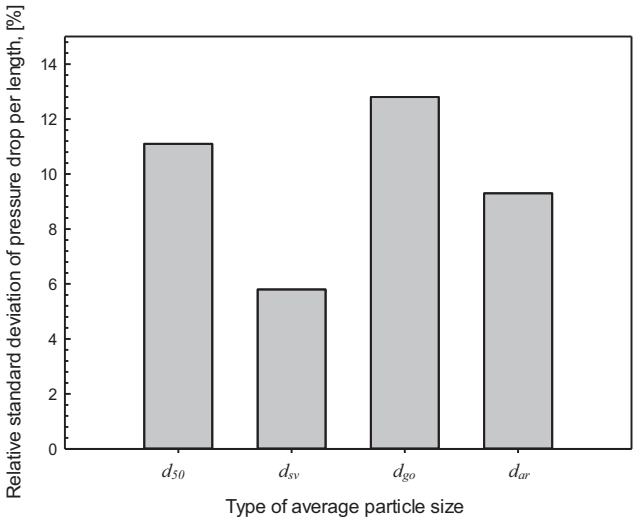


**Fig. 9.** RSD of pressure drop per length for $d_{50}$, $d_{sv}$, $d_{go}$, $d_{ar}$, respectively. Superficial gas velocity was changed from 14.8 to 30 m/s and the solid mass flow rate was fixed at 0.3 kg/s.

the solid. Since the drag force is related to the particle surface energy, the $d_{sv}$ value has been used to determine the average particle size in many fluidized bed studies [67–69]. Also, as explained in Section 4.2, in the pneumatic conveying system, the PSD variation was attributed to the acceleration of large particles by moving small particles at a high speed. The increase in the total particle surface area due to an increase in the fraction of fine particles is described in Section 4.2. Thus, $d_{sv}$ is more appropriate for the pneumatic conveying system than $d_{50}$, the mean particle size.

## 5. Conclusion

A horizontal pneumatic conveying system was analyzed via CPFD simulation in the present study. As the k value increased, the saltation velocity diminished and the pressure drop per length decreased due to an increase in average particle velocity. Based on the effect of PSD on the hydrodynamics of pneumatic conveying system, the PSD widened, leading to a rapid flow of small particles between large particles that were also accelerated. As the PSD widened, the fraction of fine particles increased together with the total particle surface area. As the total particle surface area increased, the particle area affected by air also increased, followed by an increase in the average particle velocity. The method for determining the average particle size appropriate for interpreting hydrodynamics of the pneumatic conveying system was investigated. The $d_{sv}$ was the most suitable parameter for interpreting the hydrodynamics of the pneumatic conveying system. Accordingly, the average RSD according to the PSD was 5.8%. It was established that the average RSD was 2-fold less than the value obtained with $d_{50}$ conventionally used in a pneumatic conveying system.

## Declaration of Competing Interest

The authors declare that they have no known competing financial interests or personal relationships that could have appeared to influence the work reported in this paper.

## Acknowledgement

This work was supported by a grant (No.20163010050070) from the Korea Institute of Energy Technology Evaluation and Planning (KETEP) funded by the Ministry of Trade, Industry and Energy (MOTIE), Republic of Korea.

## Appendix A. Supplementary material

Supplementary data to this article can be found online at https://doi.org/10.1016/j.apt.2021.05.010.

## References

[1] M. Güner, Pneumatic conveying characteristics of some agricultural seeds, J. Food Eng. 80 (2007) 904–913, https://doi.org/10.1016/j.jfoodeng.2006.08.010.
[2] A.H. Pelegrina, G.H. Crapiste, Modelling the pneumatic drying of food particles, J. Food Eng. 48 (2001) 301–310, https://doi.org/10.1016/S0260-8774(00)00170-9.
[3] G.E. Klinzing, A review of pneumatic conveying status, advances and projections, Powder Technol. 333 (2018) 78–90, https://doi.org/10.1016/j.powtec.2018.04.012.
[4] W.-C. Yang, Handbook of Fluidization and Fluid-Particle Systems, first ed., CRC Press, New York, 2003.
[5] D. Mills, Pneumatic Conveying Design Guide, third ed., Butterworth-Heinemann, Amsterdam, 2016.
[6] G.E. Klinzing, F. Rizk, R. Marcus, L.S. Leung, Pneumatic Conveying of Solids, Springer Netherlands, Dordrecht, 2010. https://doi.org/10.1007/978-90-481-3609-4.
[7] O. Molerus, Overview: pneumatic transport of solids, Powder Technol. 88 (1996) 309–321, https://doi.org/10.1016/S0032-5910(96)03136-1.
[8] C.G. Toomey, Pneumatic conveying system optimization, IEEE Trans. Ind. Appl. 50 (2014) 4319–4322, https://doi.org/10.1109/TIA.2014.2346695.
[9] L.M. Gomes, A.L.A. Mesquita, Effect of particle size and sphericity on the pickup velocity in horizontal pneumatic conveying, Chem. Eng. Sci. 104 (2013) 780–789, https://doi.org/10.1016/j.ces.2013.08.055.
[10] S. Matsumoto, M. Kikuta, S. Maeda, Effect of particle size on the minimum transport velocity for horizontal pneumatic conveying of solids, J. Chem. Eng. Jpn. 10 (1977) 273–279, https://doi.org/10.1252/jcej.10.273.
[11] C.P. Narimatsu, M.C. Ferreira, Vertical pneumatic conveying in dilute and dense-phase flows: experimental study of the influence of particle density and diameter on fluid dynamic behavior, Brazil. J. Chem. Eng. 18 (2001) 221–232, https://doi.org/10.1590/S0104-66322001000300002.
[12] E. Heinl, M. Bohnet, Numerical simulation of particle wall adhesion in gas-solid flows, Chem. Eng. Technol. 27 (2004) 1143–1146, https://doi.org/10.1002/ceat.200407037.
[13] S. Laín, M. Sommerfeld, Numerical calculation of pneumatic conveying in horizontal channels and pipes: detailed analysis of conveying behaviour, Int. J. Multiph. Flow 39 (2012) 105–120, https://doi.org/10.1016/j.ijmultiphaseflow.2011.09.006.
[14] E.V.P.J. Manjula, W.K.H. Ariyaratne, C. Ratnayake, M.C. Melaaen, A review of CFD modelling studies on pneumatic conveying and challenges in modelling offshore drill cuttings transport, Powder Technol. 305 (2017) 782–793, https://doi.org/10.1016/j.powtec.2016.10.026.
[15] A. Saasen, B. Dahl, K. Jødestøl, Particle size distribution of top-hole drill cuttings from norwegian sea area offshore wells, Part. Sci. Technol. 31 (2013) 85–91, https://doi.org/10.1080/02726351.2011.648824.
[16] C.A. Ratnayake, Comprehensive Scaling Up Technique for, Norwegian University of Sceince and Technology, 2005.
[17] J. Xiang, D. McGlinchey, Numerical simulation of particle motion in dense phase pneumatic conveying, Granul. Matter. 6 (2004) 167–172, https://doi.org/10.1007/s10035-004-0161-2.
[18] S.B. Kuang, K.W. Chu, A.B. Yu, Z.S. Zou, Y.Q. Feng, Computational investigation of horizontal slug flow in pneumatic conveying, Ind. Eng. Chem. Res. 47 (2008) 470–480, https://doi.org/10.1021/ie070991q.
[19] W. Pu, C. Zhao, Y. Xiong, C. Liang, X. Chen, P. Lu, C. Fan, Numerical simulation on dense phase pneumatic conveying of pulverized coal in horizontal pipe at high pressure, Chem. Eng. Sci. 65 (2010) 2500–2512, https://doi.org/10.1016/j.ces.2009.12.025.
[20] S.P. Goy, J.W. Chew, K. Hadinoto, Effects of binary particle size distribution on minimum pick-up velocity in pneumatic conveying, Powder Technol. 208 (2011) 166–174, https://doi.org/10.1016/j.powtec.2010.12.015.
[21] D.M. Snider, Three fundamental granular flow experiments and CPFD predictions, Powder Technol. 176 (2007) 36–46, https://doi.org/10.1016/j.powtec.2007.01.032.
[22] J.H. Lim, K. Bae, J.H. Shin, J.H. Kim, D.H. Lee, J.H. Han, D.H. Lee, Effect of particle-particle interaction on the bed pressure drop and bubble flow by computational particle-fluid dynamics simulation of bubbling fluidized beds with shroud nozzle, Powder Technol. 288 (2016) 315–323, https://doi.org/10.1016/j.powtec.2015.11.017.
[23] J.Y. Kim, Z.J. Li, N. Ellis, C.J. Lim, J.R. Grace, Model for attrition in sorption-enhanced chemical-looping reforming in fluidized beds, Fuel Process. Technol. 213 (2021) 106702, https://doi.org/10.1016/j.fuproc.2020.106702.
[24] X. Jiang, L. Zhou, J. Liu, X. Han, A model on attrition of quartzite particles as a bed material in fluidized beds, Powder Technol. 195 (2009) 44–49, https://doi.org/10.1016/j.powtec.2009.05.009.

[25] Y. Liang, C.Y. Guo, X. Zhao, Q. Qin, Y. Cheng, L. He, CPFD simulation on particle behaviour in an entrained-flow gasifier, Clean Energy 4 (2020) 75–84, https://doi.org/10.1093/ce/zkz032.
[26] H. Zhang, Y. Lu, A computational particle fluid-dynamics simulation of hydrodynamics in a three-dimensional full-loop circulating fluidized bed: effects of particle-size distribution, Particuology 49 (2020) 134–145, https://doi.org/10.1016/j.partic.2019.02.004.
[27] X. Zhu, P. Dong, Q. Tu, Z. Zhu, W. Yang, H. Wang, Investigation of gas-solids flow characteristics in a pressurised circulating fluidised bed by experiment and simulation, Powder Technol. 366 (2020) 420–433, https://doi.org/10.1016/j.powtec.2020.02.047.
[28] Y. Jin, H. Lu, X. Guo, X. Gong, Application of CPFD method in the simulation of vertical dense phase pneumatic conveying of pulverized coal, Powder Technol. 357 (2019) 343–351, https://doi.org/10.1016/j.powtec.2019.08.102.
[29] W.K.H. Ariyaratne, C. Ratnayake, M.C. Melaaen, Application of the MP-PIC method for predicting pneumatic conveying characteristics of dilute phase flows, Powder Technol. 310 (2017) 318–328, https://doi.org/10.1016/j.powtec.2017.01.048.
[30] A. Malagalage, W.K.H. Ariyaratne, C. Ratnayake, M.C. Melaaen, Experiments and simulations for horizontal pneumatic transport of dry drill cuttings, Chem. Eng. Technol. 41 (2018) 1531–1537, https://doi.org/10.1002/ceat.201700553.
[31] P.J. O'Rourke, D.M. Snider, A new blended acceleration model for the particle contact forces induced by an interstitial fluid in dense particle/fluid flows, Powder Technol. 256 (2014) 39–51, https://doi.org/10.1016/j.powtec.2014.01.084.
[32] F.M. Auzerais, R. Jackson, W.B. Russel, The resolution of shocks and the effects of compressible sediments in transient settling, J. Fluid Mech. 195 (1988) 437–462, https://doi.org/10.1017/S0022112088002472.
[33] C.Y. Wen, Y.H. Yu, Mechanics of fluidization, in: Chem. Eng. Prog., Symp. Ser., 1966, pp. 100–111. http://chemport.cas.org/cgi-bin/sdcgi?APP=ftslink&action=reflink&origin=wiley&version=1.0&coi=1:CAS:528:DyaF28Xks1emt7g=&md5=d8d2ec313d4de050e0d860576473472c.
[34] S. Ergun, Fluid flow through packed columns, Chem. Eng. Prog. 48 (1952) 89–94 (accessed February 7, 2019) http://ci.nii.ac.jp/naid/10003393451/en/.
[35] D. Gidaspow, Multiphase flow and fluidization: Continuum and kinetic theory description, Academic Press, San Diego, 2012. https://doi.org/10.1016/S0167-2991(13)65476-2.
[36] F. Zafiryadis, A.D. Jensen, Y. Laxminarayan, W. Lin, E.A. Hove, M.B. Larsen, H. Wu, Predicting cold gas-solid flow in a pilot-scale dual-circulating fluidized bed: validation of computational particle fluid dynamics model, Powder Technol. 381 (2021) 25–43, https://doi.org/10.1016/j.powtec.2020.11.070.
[37] J. Heintzenberg, Properties of the log-normal particle size distribution, Aerosol Sci. Technol. 21 (1994) 46–48, https://doi.org/10.1080/02786829408959695.
[38] J.Y. Kim, Jet Attrition Characteristics of Chemical Looping Oxygen Carriers and CO2 Sorbents, University of British Columbia, 2020. https://doi.org/10.14288/1.0392791.
[39] W.C. Sung, J.Y. Kim, C.K. Ko, D.H. Lee, Fine generation ratio of iron ore in the cyclone of a gas–solid circulating fluidized bed, Powder Technol. 363 (2020) 256–264, https://doi.org/10.1016/j.powtec.2019.12.042.
[40] G.D. Buchan, Applicability of the simple lognormal model to particle-size distribution in soils, Soil Sci. 147 (1989) 155–161.
[41] M. Fátima Vaz, M.A. Fortes, Grain size distribution: the lognormal and the gamma distribution functions, Scr. Metall. 22 (1988) 35–40, https://doi.org/10.1016/S0036-9748(88)80302-8.
[42] J.Y. Kim, N. Ellis, C.J. Lim, J.R. Grace, Attrition of binary mixtures of solids in a jet attrition unit, Powder Technol. 352 (2019) 445–452, https://doi.org/10.1016/j.powtec.2019.05.010.
[43] J.Y. Kim, J.W. Bae, J.R. Grace, N. Epstein, D.H. Lee, Hydrodynamic characteristics at the layer inversion point in three-phase fluidized beds with binary solids, Chem. Eng. Sci. 157 (2017) 99–106, https://doi.org/10.1016/j.ces.2015.11.021.
[44] R. Courant, K. Friedrichs, H. Lewy, Über die partiellen Differenzengleichungen der mathematischen Physik, Kurt Otto Friedrichs. (1986) 53–95, https://doi.org/10.1007/978-1-4612-5385-3_7.
[45] J. Smagorinsky, General circulation experiments with the primitive equations, Mon. Weather Rev. 91 (1963) 99–164, https://doi.org/10.1175/1520-0493(1963)091<0099:GCEWTP>2.3.CO;2.
[46] W. Wei, G. Qingliang, W. Yuxin, Y. Hairui, Z. Jiansheng, L. Junfu, Experimental study on the solid velocity in horizontal dilute phase pneumatic conveying of fine powders, Powder Technol. 212 (2011) 403–409, https://doi.org/10.1016/j.powtec.2011.06.014.
[47] K. Hong, Z. Shi, W. Wang, J. Li, A structure-dependent multi-fluid model (SFM) for heterogeneous gas-solid flow, Chem. Eng. Sci. 99 (2013) 191–202, https://doi.org/10.1016/j.ces.2013.05.050.
[48] B. Lu, W. Wang, J. Li, Searching for a mesh-independent sub-grid model for CFD simulation of gas-solid riser flows, Chem. Eng. Sci. 64 (2009) 3437–3447, https://doi.org/10.1016/j.ces.2009.04.024.
[49] C. Chen, J. Werther, S. Heinrich, H.Y. Qi, E.U. Hartge, CPFD simulation of circulating fluidized bed risers, Powder Technol. 235 (2013) 238–247, https://doi.org/10.1016/j.powtec.2012.10.014.
[50] T. McKeen, T. Pugsley, Simulation and experimental validation of a freely bubbling bed of FCC catalyst, Powder Technol. 129 (2003) 139–152, https://doi.org/10.1016/S0032-5910(02)00294-2.
[51] M. Hubert, H. Kalman, Experimental determination of length-dependent saltation velocity in dilute flows, Powder Technol. 134 (2003) 156–166, https://doi.org/10.1016/S0032-5910(03)00139-6.
[52] M. Ochi, Saltation velocity of the gas-solid twophase flow in a horizontal pipe, in: Y. Tsuji, D.E. Stock (Eds.), First ASME-JSME Fluids Eng. Conf. FED-121, American Society of Mechanical Engineers, 1991, pp. 163–166. https://books.google.co.kr/books?id=D3YeAQAAIAAJ.
[53] A. Biobaku, W. Schmitz, R. Naidoo, Evaluation and comparison of saltation velocity correlations in the context of pulverised fuel transportation, Energy 181 (2019) 694–708, https://doi.org/10.1016/j.energy.2019.05.199.
[54] F.J. Cabrejos, G.E. Klinzing, Pickup and saltation mechanisms of solid particles in horizontal pneumatic transport, Powder Technol. 79 (1994) 173–186, https://doi.org/10.1016/0032-5910(94)02815-X.
[55] H.Y. Lee, I.S. Hsu, Investigation of saltating particle motions, J. Hydraul. Eng. 120 (1994) 831–845, https://doi.org/10.1061/(ASCE)0733-9429(1994)120:7(831).
[56] J.E. Hilton, P.W. Cleary, The influence of particle shape on flow modes in pneumatic conveying, Chem. Eng. Sci. 66 (2011) 231–240, https://doi.org/10.1016/j.ces.2010.09.034.
[57] S. Fokeer, S. Kingman, I. Lowndes, A. Reynolds, Characterisation of the cross sectional particle concentration distribution in horizontal dilute flow conveying – a review, Chem. Eng. Process. Process Intensif. 43 (2004) 677–691, https://doi.org/10.1016/S0255-2701(03)00096-5.
[58] R. Kaitna, M.C. Palucis, B. Yohannes, K.M. Hill, W.E. Dietrich, Earth Surface behavior in experimental debris flows, J. Geophys. Res. Earth Surf. 121 (2016) 2298–2317, https://doi.org/10.1002/2015JF003725.
[59] P. Coussot, Mudflow Rheology and Dynamics, Routledge, 2017. https://doi.org/10.1201/9780203746349.
[60] D. Leith, Drag on nonspherical objects, Aerosol Sci. Technol. 6 (1987) 153–161, https://doi.org/10.1080/02786828708959128.
[61] C.-T. Lee, D. Leith, Drag force on agglomerated spheres in creeping flow, J. Aerosol Sci. 20 (1989) 503–513, https://doi.org/10.1016/0021-8502(89)90097-9.
[62] N. Santo, D. Portnikov, I. Eshel, R. Taranto, H. Kalman, Experimental study on particle steady state velocity distribution in horizontal dilute phase pneumatic conveying, Chem. Eng. Sci. 187 (2018) 354–366, https://doi.org/10.1016/j.ces.2018.04.058.
[63] H.M. Parsons, D.R. Ekman, T.W. Collette, M.R. Viant, Spectral relative standard deviation: a practical benchmark in metabolomics, Analyst 134 (2009) 478–485, https://doi.org/10.1039/b808986h.
[64] J. Sauter, The determination of the size of fuel particles, Vdi-Forschungsh. Nr. 279 (70) (1926) 1040–1042.
[65] D. Wang, L.-S. Fan, Particle characterization and behavior relevant to fluidized bed combustion and gasification systems, in: Fluid. Bed Technol. Near-Zero Emiss. Combust. Gasif., Elsevier, 2013, pp. 42–76. https://doi.org/10.1533/9780857098801.1.42.
[66] P.B. Kowalczuk, J. Drzymala, Physical meaning of the Sauter mean diameter of spherical particulate matter, Part. Sci. Technol. 34 (2016) 645–647, https://doi.org/10.1080/02726351.2015.1099582.
[67] J.Y. Kim, N. Ellis, C.J. Lim, J.R. Grace, Effect of calcination/carbonation and oxidation/reduction on attrition of binary solid species in sorption-enhanced chemical looping reforming, Fuel 271 (2020) 117665, https://doi.org/10.1016/j.fuel.2020.117665.
[68] K. Bae, J.H. Lim, J.-H. Kim, D.-H. Lee, J.-H. Han, S.-H. Park, D.H. Lee, Bubble characteristics by pressure fluctuation analysis in gas-solid bubbling fluidized beds with or without internal, Korean J. Chem. Eng. 34 (2017) 566–573, https://doi.org/10.1007/s11814-016-0255-7.
[69] J.Y. Kim, J.W. Bae, J.R. Grace, N. Epstein, D.H. Lee, Horizontal immersed heater-to-bed heat transfer with layer inversion in gas-liquid-solid fluidized beds of binary solids, Chem. Eng. Sci. 170 (2017) 501–507, https://doi.org/10.1016/j.ces.2017.01.007.